IEEE Access
Multidisciplinary | Rapid Review | Open Access Journal

Received August 1, 2021, accepted August 17, 2021, date of publication August 24, 2021, date of current version August 30, 2021.

Digital Object Identifier 10.1109/ACCESS.2021.3107419

KM Learning for Millimeter-Wave Beam Alignment and Tracking: Predictability and Interpretability

QIYOU DUAN[1], TAEJOON KIM[2], (Senior Member, IEEE), AND HADI GHAUCH[3], (Member, IEEE)

[1]Department of Electrical Engineering, City University of Hong Kong, Hong Kong
[2]Department of Electrical Engineering and Computer Science, The University of Kansas, Lawrence, KS 66045, USA
[3]Department of COMELEC, Telecom ParisTech, 75013 Paris, France

Corresponding author: Qiyou Duan (qyduan.ee@my.cityu.edu.hk)

The work of Taejoon Kim was supported in part by the National Science Foundation (NSF) under Grant CNS1955561, and in part by the Office of Naval Research (ONR) under Grant N00014-21-1-2472.

ABSTRACT A data representation technique dubbed Kolmogorov model (KM), has been applied to the beam alignment problem in large-dimensional antenna systems. The previous learning-based beam alignment solely focused on utilizing the predictive power of KM, i.e., the capability of predicting the outcome of random variables that are outside the training set, to reduce the beam training overhead. However, a distinctive feature of KM, namely, the interpretability which enables the capability of extracting additional information hidden inside the data, has not yet been exploited. Moreover, the prohibitively high computational complexity of the existing KM learning algorithm offsets the benefits brought by KM and hampers its application to large-scale problems. In this paper, we propose a joint beam alignment and tracking framework by incorporating the predictability and interpretability of KM. Especially, our proposed scheme enables a novel interpretable beam tracking that reveals insights on relations among the sounded observations to alleviate the beam sounding overhead after the initial beam alignment. To reduce the computational complexity of KM learning, two enhancement approaches, based on discrete monotonic optimization (DMO) and dual optimization, respectively, are proffered. Numerical results demonstrate that the proposed methods can reduce the computational cost of the existing KM learning algorithm by up to three orders of magnitude. Furthermore, the proposed methods show superior beam alignment and tracking performance over other state-of-the-art techniques, notably in the low signal-to-noise ratio (SNR) regime.

INDEX TERMS Beam tracking, Kolmogorov model (KM), discrete monotonic optimization (DMO), dual optimization, predictability, interpretability, low latency.

I. INTRODUCTION

At the millimeter-wave (mmWave) spectrum, radio propagation suffers from severe path loss and atmospheric impairments that are compensated for by using large antenna arrays to produce directional narrow beams [1]–[3]. The so called ''beam alignment'' procedure, which finds the best transmit-and-receive beam pair without estimating the channel state information (CSI), is required to establish an available communication link. A straightforward approach to the beam alignment problem is exhaustive beam search, also known as beam sweeping, which sequentially scans the entire beam space. However, the overall training overhead is indeed prohibitive due to the large size of beam codebooks in mmWave massive multiple-input multiple-output (MIMO) communication systems, offsetting the benefits of the abundant bandwidth of mmWave that promises a higher channel capacity [4], [5].

To reduce the overhead of exhaustive beam search, various approaches have been proposed in the past decade. The hierarchical codebooks, which typically consist of a small number of low-resolution wide beams at the upper layer of the codebook and a large number of high-resolution narrow beams at the lower layer of the codebook, were

The associate editor coordinating the review of this manuscript and approving it for publication was Wei Liu.

proposed [1], [6], [7]. Other methods fallen into the same ''structured beam alignment'' paradigm include beam coding [8], [9], overlapped beam patterns [10], [11], and compressed sensing-based algorithms [12]–[17]. Despite a battery of such beam alignment techniques, there still remains a challenge of further reducing the beam training overhead especially when the mobility and link blockage are considered.

While the reliability of initial beam alignment in mmWave is well-understood, directional narrow beams for data transmission, especially in mobile urban networks, can put beamforming gain in peril [18]–[20]. Due to mobility, frequent misalignment and blockages require repeated beam alignment, which further lead to enormous overhead and performance degradation. To be specific, the higher the mobility of users, the more frequent the misalignment and blockage events occur [21]. To remedy, the more resources are needed to be allocated to maintain beam alignment. Additionally, reliable operation at low signal-to-noise ratio (SNR) is critical for mmWave communication systems that are limited by heavy mixed signal processing with an excessive power consumption. Thus, it is of great importance to explore efficient methods capable of mitigating the beam sounding overhead under mobility while exhibiting reliable performance in the low SNR regime.

With the rapid development of the cutting-edge hardware devices and signal processing units, the capability of high performance computing makes the appealing machine learning-based techniques possible to be applied to practical wireless communication systems. Recently, a Kolmogorov model (KM) learning-based beam alignment technique, motivated by a data representation of binary random variables, was introduced [22], [23]. In particular, the quality of beam pairs was modeled by a double-index set of binary random variables based on the received signal power. The learning of KM parameters was formulated as a coupled combinatorial optimization problem, which can then be decomposed into two subproblems including the linearly-constrained quadratic program (LCQP) and binary quadratic program (BQP). A block coordinate descent (BCD) method was adopted to iterate between the two subproblems in an alternative manner. An elegant, low-complexity Frank-Wolfe (FW) algorithm [24] was used to optimally solve the LCQP by exploiting structure of the unit probability simplex. Meanwhile, the BQP problem was handled by employing a semi-definite relaxation with randomization (SDRwR) method [25]. However, the high computational complexity of the latter prevents it from being applied to the system equipped with large-dimensional array antennas. It is thus critical to find more efficient and fast KM learning algorithms that are readily applicable to large-scale problems. Moreover, the previous work only focused on the predictability (the capability of predicting the outcome of random variables that are outside the training set) in terms of reducing the beam alignment overhead. Unfortunately, a distinctive advantage of KM, i.e., the interpretability (the capability of extracting additional information or insights that are hidden inside the data) has not yet been exploited.

In this work, we leverage both the predictability and interpretability of KM to enable low-latency beam alignment and tracking for mmWave communication systems. The proposed predictive beam alignment combined with interpretable beam tracking can achieve a significantly reduced beam training overhead. To be specific, the predictive power of the KM plays an essential role in improving link connectivity by only utilizing a subsampled beam set whose cardinality is smaller than that of the entire beam codebook. After the initial beam alignment, we predict future beam switching directions and further narrow down the beam search procedure to few likely beams by exploiting the interpretability of KM, thus avoiding the enormous cost for beam tracking.

Moreover, in order to address the impractically high computational complexity of the existing KM learning algorithm relying on SDRwR [22], [26], we propose two enhanced solvers in resolving the BQP subproblem of KM learning in a more efficient way. In particular, discrete monotonic optimization (DMO) and dual optimization are leveraged. We demonstrate numerically that the proposed KM learning methods can achieve comparable beam alignment performance with a significantly reduced computational cost, compared to the existing KM learning algorithm [26]. It is also shown that the proposed methods by incorporating the predictability and interpretability of KM outperform the benchmarks in terms of both the beam tracking overhead and achievable throughput. Finally, the robustness of the proposed methods in the low SNR regime is validated by simulation results.

The rest of the paper is organized as follows. Section II introduces the concept of KM and system model. In Section III, the joint scheme of predictive beam alignment and interpretable beam tracking is elaborated. We provide two enhanced optimization-based methods for KM learning in Section IV. Section V presents the numerical results. The conclusions are finally given in Section VI.

Notations: A bold capital letter $\mathbf{A}$ is a matrix, a bold lowercase letter $\mathbf{a}$ is a vector, and a calligraphic capital letter $\mathcal{A}$ is a set with cardinality $|\mathcal{A}|$. $(\cdot)^T$, $(\cdot)^*$, $\lfloor\cdot\rfloor$, and $\lceil\cdot\rceil$ are the transpose, conjugate transpose, floor and ceiling operators, respectively. a_i, $\mathbf{a}_{i:j} \triangleq [a_i, \cdots, a_j]^T$ $(1 \leq i < j \leq N)$, $\|\mathbf{a}\|_2$, and $\text{supp}(\mathbf{a}) \triangleq \{i|a_i \neq 0, i \in \{1, \ldots, N\}\}$ are the ith element, subvector, ℓ_2-norm, and the support set of $\mathbf{a} \in \mathbb{C}^N$, respectively. $\text{rank}(\mathbf{A})$, $\text{trace}(\mathbf{A})$, $\text{diag}(\mathbf{A})$, and $\|\mathbf{A}\|_F$ represent the rank, trace, main diagonal elements, and the Frobenius norm of $\mathbf{A}$, respectively. $\langle \mathbf{A}, \mathbf{B} \rangle = \text{trace}(\mathbf{A}^T\mathbf{B})$ denotes the Frobenius inner product of matrices $\mathbf{A}$ and $\mathbf{B}$ with the same size, and $\mathbf{A} \succeq \mathbf{0}$ indicates that $\mathbf{A}$ is positive semi-definite (PSD). For $\mathbf{A} \in \mathbb{R}^{N\times N}$, $\lambda_i(\mathbf{A})$ is the ith eigenvalue of $\mathbf{A}$, $i = 1, \ldots, N$. $\mathbb{R}_+^N$, $\mathbb{B}^N$, and $\mathbb{S}^{N\times N}$ denote the nonnegative real-valued $N\times 1$ vector space, $N\times 1$ binary vector space with each entry chosen from $\{1, 0\}$, and $N\times N$ symmetric matrix space, respectively. $\mathcal{N}(\mu, \sigma^2)$ and $\mathcal{CN}(\mu, \sigma^2)$ are the Gaussian and complex Gaussian distributions with mean μ and variance σ^2,

respectively. $\mathbf{I}_N$ is the $N\times N$ identity matrix and $\mathbf{e}_i$ denotes the ith column of the identity matrix of appropriate size. $\mathbf{1}$ and $\mathbf{0}$ are all-one and all-zero column vectors, respectively. Finally, $\mathbb{I}(E)$ is the indicator function that takes value 1 when the event E happens and value 0 otherwise, and $E_1 \Rightarrow E_2$ means that one outcome/event (E_1) implies another one (E_2).

II. PRELIMINARIES AND SYSTEM MODEL

The concept of KM and some preliminaries are first introduced. The beam alignment and tracking system model of mmWave MIMO communications is then presented.

A. KOLMOGOROV MODEL

Prior to introducing the KM of a binary random variable, we review the fundamentals of Kolmogorov probability theory by defining a measurable probability space [27].

Definition 1: A probability space $(\Omega, \mathcal{E}, P)$ is a triple formed by the sample space Ω, the event space $\mathcal{E}$ consisting of the subsets of Ω, and a probability measure P defined on $(\Omega, \mathcal{E})$. $P(E)$ assigns a probability to the event $E \in \mathcal{E}$ such that the following conditions hold: i) $P(E) \geq 0, \forall E \in \mathcal{E}$ (nonnegativity), ii) $P(\Omega) = 1$ (normalization), and iii) $P(\cup_{i=1}^{\infty} E_i) = \sum_{i=1}^{\infty} P(E_i)$ for the disjoint events $E_i \in \mathcal{E}, \forall i$ (countable additivity).

A double-index set of binary random variables $X_{t,r} \in \mathcal{X} \triangleq \{1, 0\}, \forall (t, r) \in \mathcal{S}$, is considered, where $\mathcal{X}$ is the binary alphabet of $X_{t,r}$ and $\mathcal{S}$ denotes the set of all index pairs. The set Ω, also known as the space of elementary events, is defined as $\Omega \triangleq \{\omega_d | d = 1, \ldots, D\}$, where ω_d denotes an individual elementary event and D is the dimension of Kolmogorov space. Let $\Pr(X_{t,r} = \mathcal{X}(x)) \in [0, 1]$ be the probability that the event $X_{t,r} = \mathcal{X}(x)$ occurs, where x denotes the index of $\mathcal{X}$, i.e., $\mathcal{X}(1) = 1$ and $\mathcal{X}(2) = 0$. By Definition 1, the probability of two realizations of $X_{t,r}$ ($X_{t,r} = 1$ or $X_{t,r} = 0$) can be expressed as

$$\Pr\left(X_{t,r} = \mathcal{X}(x)\right) = P\left(X_{t,r}^{-1}(\{\mathcal{X}(x)\})\right) = \sum_{\omega_d \in X_{t,r}^{-1}(\{\mathcal{X}(x)\})} P(\omega_d), \; x \in \{1, 2\}, \quad (1)$$

where $X_{t,r}^{-1}(\{\mathcal{X}(x)\}) \triangleq \{\omega_d \in \Omega | X_{t,r} = \mathcal{X}(x)\}$ is the inverse image of the event $X_{t,r} = \mathcal{X}(x)$. Since $X_{t,r}$ is binary, the following holds $\Pr(X_{t,r} = 1) + \Pr(X_{t,r} = 0) = 1$. Without loss of generality, it suffices to focus on one outcome, for instance, $X_{t,r} = 1$. By (1), the KM [26], [28] of $X_{t,r}$ is given by

$$\Pr(X_{t,r} = 1) = \boldsymbol{\theta}_t^T \boldsymbol{\psi}_r, \; \forall (t, r) \in \mathcal{S}, \quad (2)$$

where $\boldsymbol{\theta}_t \triangleq [P(\omega_1), \cdots, P(\omega_D)]^T \in \mathbb{R}_+^D$ is the probability mass function vector and $\boldsymbol{\psi}_r \triangleq [\psi_{r,1}, \cdots, \psi_{r,D}]^T \in \mathbb{B}^D$ is the binary indicator vector with each entry being

$$\psi_{r,d} = \begin{cases} 1, & \text{if } \omega_d \in X_{t,r}^{-1}(\{\mathcal{X}(1)\}) \\ 0, & \text{otherwise,} \end{cases} \quad d = 1, \ldots, D.$$

In particular, $\boldsymbol{\theta}_t$ is in the unit probability simplex $\mathcal{P} \triangleq \{\mathbf{p} \in \mathbb{R}_+^D | \mathbf{1}^T \mathbf{p} = 1\}$, i.e., $\boldsymbol{\theta}_t \in \mathcal{P}$, and $\boldsymbol{\psi}_r$ denotes the support set of $X_{t,r}$ (associated with the case when $X_{t,r} = 1$). In addition, note that $\Pr(X_{t,r} = 0) = \boldsymbol{\theta}_t^T (\mathbf{1} - \boldsymbol{\psi}_r)$.

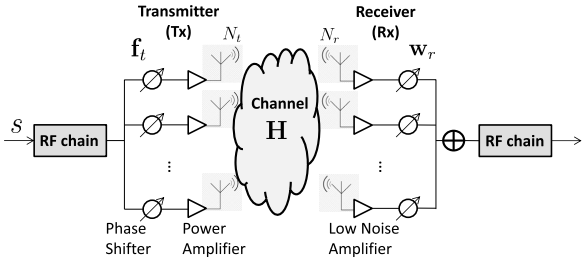

FIGURE 1. Diagram of the mmWave MIMO system with a fully analog architecture.

B. MILLIMETER-WAVE MIMO SYSTEM MODEL

We consider a mmWave MIMO communication system, as depicted in Fig. 1, where the transmitter and receiver are equipped with N_t and N_r antennas, respectively. A single radio-frequency (RF) chain is employed at both the transmitter and receiver, and thus the analog beamforming/combining is adopted. A narrow-band block fading channel is assumed with a coherence interval being T channel uses. During a coherence block, as shown in Fig. 2, the initial K^τ channel uses are utilized to find the best beamformer-combiner pair (i.e., the beam alignment/tracking phase) and the remaining $T - K^\tau$ channel uses are set aside for data communication via the well-aligned beam pair (i.e., the data transmission phase), where τ denotes the channel block index. In particular, after the initial beam alignment, a beam tracking procedure is necessary to maintain or adjust the well-aligned beam pair by considering the beam switching and channel evolution.

In the beam alignment phase, the transmitter chooses an analog beamformer $\mathbf{f}_t \in \mathbb{C}^{N_t \times 1}$ from the transmit beam sounding codebook $\mathcal{F}$ ($\mathbf{f}_t \in \mathcal{F}$), while the receiver selects an analog combiner $\mathbf{w}_r \in \mathbb{C}^{N_r \times 1}$ from the receive beam sounding codebook $\mathcal{W}$ ($\mathbf{w}_r \in \mathcal{W}$). Let $\mathcal{I}_\mathcal{F}$ and $\mathcal{I}_\mathcal{W}$ denote the index sets of the predefined codebooks $\mathcal{F}$ and $\mathcal{W}$, respectively, with cardinalities $|\mathcal{I}_\mathcal{F}|$ and $|\mathcal{I}_\mathcal{W}|$. $\mathbf{f}_t$ and $\mathbf{w}_r$ satisfy the constant modulus constraint, i.e., $\|\mathbf{f}_t\|_2 = \|\mathbf{w}_r\|_2 = 1$.

Let $s \in \mathbb{C}$ be the transmitted training symbol with unit power. The received signal at channel block τ, $y_{t,r}^\tau \in \mathbb{C}$, can be expressed as (the channel block index τ is omitted for conciseness)

$$y_{t,r} = \mathbf{w}_r^* \mathbf{H} \mathbf{f}_t s + \mathbf{w}_r^* \mathbf{n}, \quad (3)$$

where $\mathbf{H} \in \mathbb{C}^{N_r \times N_t}$ is the channel matrix and $\mathbf{n} \in \mathbb{C}^{N_r \times 1}$ is the additive complex white Gaussian noise vector with each entry independently and identically distributed (i.i.d.) as zero mean and σ_n^2 variance according to $\mathcal{CN}(0, \sigma_n^2)$. It is noted that the SNR is $1/\sigma_n^2$, and we can further define the received SNR as $\eta \triangleq |\mathbf{w}_r^* \mathbf{H} \mathbf{f}_t|^2 / \sigma_n^2$, where $|\mathbf{w}_r^* \mathbf{H} \mathbf{f}_t|^2$ denotes the beamforming gain. The beam alignment problem, which is to find the optimal beam pair by maximizing the beamforming gain, can

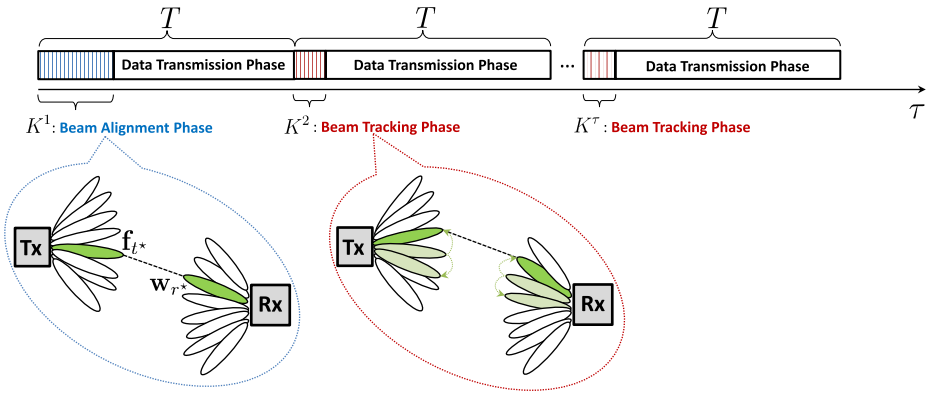

FIGURE 2. Illustration of the beam alignment/tracking during multiple channel blocks.

be formulated as

$$\max_{\mathbf{f}_t,\mathbf{w}_r} |\mathbf{w}_r^*\mathbf{H}\mathbf{f}_t|^2 \quad \text{s.t. } \mathbf{f}_t \in \mathcal{F}, \mathbf{w}_r \in \mathcal{W}. \tag{4}$$

However, it is not practical for the receiver to calculate the beamforming gain in (4) directly due to the lack of CSI. Instead, the problem in (4) can be approximated by using the received signal power as

$$\max_{\mathbf{f}_t,\mathbf{w}_r} \{\gamma_{t,r} \triangleq |y_{t,r}|^2\} \quad \text{s.t. } \mathbf{f}_t \in \mathcal{F}, \mathbf{w}_r \in \mathcal{W}. \tag{5}$$

It is worth noting that, under the fully analog beamforming architecture, the best transmit-receive beam pair is found by solving the beam alignment problem in (5). This is different from the hybrid analog-digital precoding and combining scenario where the estimated CSI is required at both the transmitter and receiver [6], [13]–[15], [17]. A straightforward approach to solving (5) is the exhaustive beam search, which requires both the transmitter and receiver to scan the entire beam space ($\mathcal{F}$ and $\mathcal{W}$). Unfortunately, this exhaustive search method incurs a training overhead of $|\mathcal{S}| = |\mathcal{I}_\mathcal{F}\times\mathcal{I}_\mathcal{W}|$ (whose sampling rate is 100%), which indeed overwhelms the available channel coherence resources due to the large size of codebooks ($|\mathcal{I}_\mathcal{F}|$ and $|\mathcal{I}_\mathcal{W}|$) in mmWave massive MIMO systems.

To address this issue, a KM learning-based beam alignment was proposed by utilizing the predictive power of KM [22], [23]. It was motivated by the fact that the double-index random variable $X_{t,r}$ in (2) can represent any two-dimensional learning applications (involving matrices). We will review the existing predictive beam alignment scheme in Section III-A.

III. KM LEARNING-BASED FRAMEWORK

The KM learning-based framework by incorporating the predictive beam alignment and interpretable beam tracking is elaborated in this section.

A. PREDICTIVE BEAM ALIGNMENT

The "good" or "poor" condition of the beam pair $(\mathbf{f}_t, \mathbf{w}_r)$ for $(t, r) \in \mathcal{S} \triangleq \{(t, r)|(t, r) \in \mathcal{I}_\mathcal{F}\times\mathcal{I}_\mathcal{W}\}$, where $\mathcal{S}$ contains all beam pair indices of the transmit-and-receive joint codebook, can be modeled by using the binary random variable $X_{t,r}$ of KM in (2) as

$$\begin{cases} \Pr(\gamma_{t,r} \geq \delta) = \Pr(X_{t,r} = 1) = \boldsymbol{\theta}_t^T \boldsymbol{\psi}_r, & \text{"good"} \\ \Pr(\gamma_{t,r} < \delta) = \Pr(X_{t,r} = 0) = \boldsymbol{\theta}_t^T (\mathbf{1} - \boldsymbol{\psi}_r), & \text{"poor"}, \end{cases} \tag{6}$$

where $\delta > 0$ is a predesigned threshold value for the received signal power $\gamma_{t,r}$. To be specific, the beam pair $(\mathbf{f}_t, \mathbf{w}_r)$ is regarded as being well-aligned if $\gamma_{t,r} \geq \delta$.

In contrast to the exhaustive beam search, the KM learning-based beam alignment only uses a subset of codebook $\mathcal{K} \triangleq \{(t, r)|t \in \mathcal{I}_\mathcal{F}^{\text{train}} \subseteq \mathcal{I}_\mathcal{F}, r \in \mathcal{I}_\mathcal{W}^{\text{train}} \subseteq \mathcal{I}_\mathcal{W}\} \subset \mathcal{S}$ (also known as the training set). Let $p_{t,r}$ be the empirical probability of the beam pair $(\mathbf{f}_t, \mathbf{w}_r)$ being well-aligned. Obtaining $\{p_{t,r}\}$ for the training set $\mathcal{K}$ is a prerequisite for the KM learning-based beam alignment. Frequency estimation (FE) was proposed by estimating $\{p_{t,r}\}$, $\forall(t, r) \in \mathcal{K}$, over a time-slot interval T_{FE} [22]. Let $y_{t,r}^{(t_{\text{FE}})} = \mathbf{w}_r^*\mathbf{H}\mathbf{f}_t s + \mathbf{w}_r^*\mathbf{n}^{(t_{\text{FE}})}$ be the received signal by sounding the beam pair $(\mathbf{f}_t, \mathbf{w}_r)$ at time slot t_{FE} during a coherent channel block, the received signal power is then provided as

$$\gamma_{t,r}^{(t_{\text{FE}})} = \left|y_{t,r}^{(t_{\text{FE}})}\right|^2, \ t_{\text{FE}} \in \{1, \ldots, T_{\text{FE}}\}, \ \forall(t, r) \in \mathcal{K}.$$

The final estimate of $p_{t,r}$, attained by counting the number of events in which the condition $\gamma_{t,r}^{(t_{\text{FE}})} \geq \delta$ holds, is given by

$$p_{t,r} \approx p_{t,r}^{(T_{\text{FE}})} \triangleq \frac{1}{T_{\text{FE}}} \sum_{t_{\text{FE}}=1}^{T_{\text{FE}}} \mathbb{I}(\gamma_{t,r}^{(t_{\text{FE}})} \geq \delta), \ \forall(t, r) \in \mathcal{K}. \tag{7}$$

It is worth noting that the approximation in (7) becomes tight as T_{FE} increases.

Given the constructed training set (of empirical probabilities), the KM learning-based beam alignment, composed of training, prediction, and selection, is presented as follows.

1) TRAINING

The KM-based beam training proceeds to optimize $\{\boldsymbol{\theta}_t\}$ and $\{\boldsymbol{\psi}_r\}$ by solving the ℓ_2-norm minimization problem:

$$\{\boldsymbol{\theta}_t^\star\}, \{\boldsymbol{\psi}_r^\star\} = \underset{\{\boldsymbol{\theta}_t\},\{\boldsymbol{\psi}_r\}}{\operatorname{argmin}} \sum_{(t,r)\in\mathcal{K}} (\boldsymbol{\theta}_t^T \boldsymbol{\psi}_r - p_{t,r})^2 \quad \text{s.t. } \boldsymbol{\theta}_t \in \mathcal{P},\ \boldsymbol{\psi}_r \in \mathbb{B}^D, \forall (t,r) \in \mathcal{K}. \tag{8}$$

To deal with the coupled combinatorial nature of (8), a BCD method was proposed by dividing the problem in (8) into two subproblems: i) LCQP for $\forall t \in \mathcal{I}_{\mathcal{F}}^{\text{train}}$:

$$\boldsymbol{\theta}_t^{(\upsilon+1)} = \underset{\boldsymbol{\theta}_t\in\mathcal{P}}{\operatorname{argmin}}\, \boldsymbol{\theta}_t^T \mathbf{Q}_t^{(\upsilon)} \boldsymbol{\theta}_t - 2\boldsymbol{\theta}_t^T \mathbf{w}_t^{(\upsilon)} + \varrho_t, \tag{9}$$

where $\mathbf{Q}_t^{(\upsilon)} \triangleq \sum_{r\in\mathcal{I}_t} \boldsymbol{\psi}_r^{(\upsilon)} \boldsymbol{\psi}_r^{(\upsilon)^T}$, $\mathbf{w}_t^{(\upsilon)} \triangleq \sum_{r\in\mathcal{I}_t} \boldsymbol{\psi}_r^{(\upsilon)} p_{t,r}$, $\varrho_t \triangleq \sum_{r\in\mathcal{I}_t} p_{t,r}^2$, $\mathcal{I}_t \triangleq \{r|(t,r) \in \mathcal{K}\}$, and υ is the index of BCD iterations, and ii) BQP for $\forall r \in \mathcal{I}_{\mathcal{W}}^{\text{train}}$:

$$\boldsymbol{\psi}_r^{(\upsilon+1)} = \underset{\boldsymbol{\psi}_r\in\mathbb{B}^D}{\operatorname{argmin}}\, \boldsymbol{\psi}_r^T \mathbf{S}_r^{(\upsilon+1)} \boldsymbol{\psi}_r - 2\boldsymbol{\psi}_r^T \mathbf{v}_r^{(\upsilon+1)} + \rho_r, \tag{10}$$

where $\mathbf{S}_r^{(\upsilon+1)} \triangleq \sum_{t\in\mathcal{I}_r} \boldsymbol{\theta}_t^{(\upsilon+1)} \boldsymbol{\theta}_t^{(\upsilon+1)^T}$, $\mathbf{v}_r^{(\upsilon+1)} \triangleq \sum_{t\in\mathcal{I}_r} \boldsymbol{\theta}_t^{(\upsilon+1)} p_{t,r}$, $\rho_r \triangleq \sum_{t\in\mathcal{I}_r} p_{t,r}^2$, and $\mathcal{I}_r \triangleq \{t|(t,r) \in \mathcal{K}\}$. By exploiting the fact that the optimization in (9) was carried out over the unit probability simplex $\mathcal{P}$, a simple iterative FW algorithm was used to optimally solve (9), while the SDRwR was employed to asymptotically solve the BQP in (10) [26].

2) PREDICTION

The trained KM parameters $\{\boldsymbol{\theta}_t^\star\}$, $\{\boldsymbol{\psi}_r^\star\}$ are utilized to predict probabilities over a test set $\mathcal{T}$ (a set of beam pairs that are not sounded) as

$$\hat{p}_{t,r} \triangleq \boldsymbol{\theta}_t^{\star T} \boldsymbol{\psi}_r^\star,\ \forall (t,r) \in \mathcal{T}, \tag{11}$$

where $\mathcal{T} \cap \mathcal{K} = \phi$ and $\mathcal{T} \cup \mathcal{K} = \mathcal{S}$.

3) SELECTION

The optimal beam pair with the highest probability of being well-aligned is selected by evaluating both the training and test sets ($\mathcal{K} \cup \mathcal{T}$) as

$$(t^\star, r^\star) = \underset{(t,r)\in\mathcal{S}}{\operatorname{argmax}} \{\hat{p}_{t,r} = \boldsymbol{\theta}_t^{\star T} \boldsymbol{\psi}_r^\star\}. \tag{12}$$

Based on the above three key steps, an overall KM learning-based beam alignment procedure is provided in Algorithm 1.

Note that, the predictability of KM was exploited to reduce the beam training overhead by using a subsampled codebook. However, the existing KM learning method relying on SDRwR to solve (10) suffers from a high computational complexity ($\mathcal{O}(D^{4.5})$) and is thereby difficult to be applied to large-scale antenna-array systems [22], [26]. In particular, the LCQP subproblem in (9), which can be solved by the FW algorithm at the negligible cost of searching for the minimum of an array ($\mathcal{O}(D)$), has been well-studied [24], while resolving the BQP subproblem in (10) introduces a major computational bottleneck. This calls for more efficient KM learning methods, which we will present in Section IV.

Algorithm 1 Overall KM Learning-Based Beam Alignment

Input: $\mathcal{F}, \mathcal{W}, \mathcal{K}, \mathcal{I}_{\mathcal{F}}^{\text{train}}, \mathcal{I}_{\mathcal{W}}^{\text{train}}, D, \delta, T_{\text{FE}}$, and I_{BCD}. Initialize $\{\boldsymbol{\psi}_r^{(1)} \in \mathbb{B}^D\}_{r\in\mathcal{I}_{\mathcal{W}}^{\text{train}}}$.
Output: $(t^\star, r^\star)$.

```
Estimate the empirical probabilities for K via FE:
for each t_FE = 1, ..., T_FE do
    for each beam pair index (t, r) ∈ K do
        Train the beam pair (f_t, w_r) and obtain γ_{t,r}^{(t_FE)}.
    end for
end for
Compute {p_{t,r}} according to (7).
Learn the KM parameters:
for υ = 1, ..., I_BCD do
    i) Update θ_t^{(υ)} for t ∈ I_F^train;
    ii) Update ψ_r^{(υ)} for r ∈ I_W^train.
end for
Obtain the final estimate {θ_t^⋆ = θ_t^{(I_BCD)}, ψ_r^⋆ = ψ_r^{(I_BCD)}}.
Calculate the predicted probability for the beam pairs which are not trained yet based on (11).
Determine the optimal beam pair according to (12).
return (t^⋆, r^⋆).
```

B. INTERPRETABLE BEAM TRACKING

The next challenge after the initial beam alignment is to update/adjust the aligned beam pair to maintain the availability of the link, i.e., the beam tracking phase ($\tau > 1$) as illustrated in Fig. 2. However, the enormous overhead induced by frequent beam realignment often makes the system unbearable. Thus, the design of schemes that alleviate the beam tracking overhead is of great importance.

To this end, a distinctive feature of KM, namely, the interpretability, extracting insights that hidden inside the data based on sounded observations, can be exploited. The following theorem provides a basis for the interpretable beam tracking.

Theorem 1 (Logical Relation Mining): Suppose two random events '$\gamma_{t,r_1} \geq \delta$' and '$\gamma_{t,r_2} \geq \delta$', whose KMs are given by $\Pr(\gamma_{t,r_1} \geq \delta) = \Pr(X_{t,r_1} = 1) = \boldsymbol{\theta}_t^T \boldsymbol{\psi}_{r_1}$ and $\Pr(\gamma_{t,r_2} \geq \delta) = \Pr(X_{t,r_2} = 1) = \boldsymbol{\theta}_t^T \boldsymbol{\psi}_{r_2}$, respectively. If the support sets of $\boldsymbol{\psi}_{r_1}$ and $\boldsymbol{\psi}_{r_2}$ satisfy the inclusion relation $\text{supp}(\boldsymbol{\psi}_{r_2}) \subseteq \text{supp}(\boldsymbol{\psi}_{r_1})$, then the following two logical relations hold:

$$\gamma_{t,r_1} \geq \delta \Rightarrow \gamma_{t,r_2} \geq \delta\ (X_{t,r_1} = 1 \Rightarrow X_{t,r_2} = 1), \tag{13}$$

$$\gamma_{t,r_2} < \delta \Rightarrow \gamma_{t,r_1} < \delta\ (X_{t,r_2} = 0 \Rightarrow X_{t,r_1} = 0). \tag{14}$$

Proof: See Appendix A.

Theorem 1 can be translated as: Given that the support set of $\boldsymbol{\psi}_{r_1}$ includes that of $\boldsymbol{\psi}_{r_2}$, if the beam pair index (t, r_1) is good, then it logically implies that the beam pair index (t, r_2) is also good. Conversely, if the beam pair index (t, r_2) is bad, then it logically implies that the beam pair index (t, r_1) is bad either. The above information can be leveraged to reduce the beam tracking overhead.

Suppose the beam training set (subsampled codebook) for beam alignment/tracking at τth channel block is $\mathcal{K}^\tau$ with

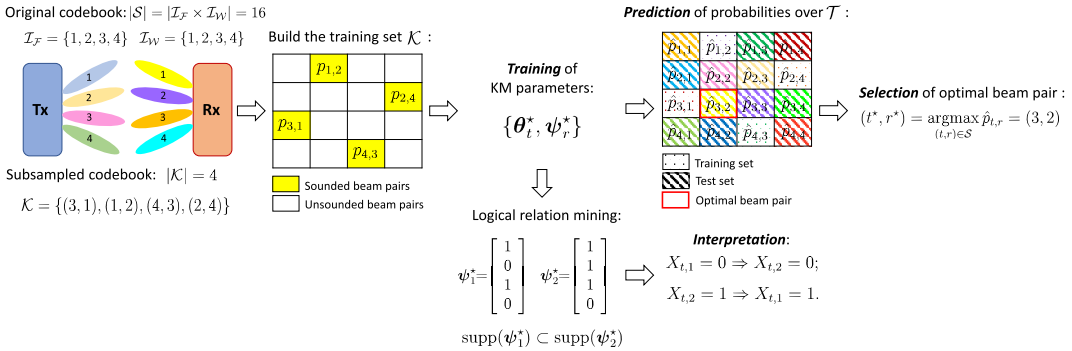

FIGURE 3. Diagram of the KM learning-based beam alignment framework: a toy example ($N_t = N_r = |\mathcal{I}_\mathcal{F}| = |\mathcal{I}_\mathcal{W}| = 4$ and $D = 4$).

$|\mathcal{K}^\tau| = K^\tau$. Let $\{\boldsymbol{\psi}_r^{\star,\tau}\}$ denote the set of learned binary indicator vectors of KM at τth channel block. We first identify a set of critical beam pair indices based on the empirical probabilities at current channel block, associated with a transmit beam index t, as

$$\mathcal{C}_t^\tau = \{(t, r_i) | p_{t,r_i}^\tau \geq \alpha\}, \tag{15}$$

where p_{t,r_i}^τ denotes the empirical probability of the beam pair index (t, r_i) at τth channel block and $\alpha \in [0, 1]$ is a threshold. By exploiting the interpretability of KM, especially via logical relation mining in Theorem 1, we obtain an expanded set of critical beam pair indices as

$$\hat{\mathcal{C}}_t^\tau = \bigcup_{i=1}^{|\mathcal{C}_t^\tau|} \{(t, r_j) | \text{supp}(\boldsymbol{\psi}_{r_j}^{\star,\tau}) \subseteq \text{supp}(\boldsymbol{\psi}_{r_i}^{\star,\tau}), (t, r_i) \in \mathcal{C}_t^\tau\}, \tag{16}$$

which encapsulates all potential good beam pair indices for a fixed t. Moreover, by considering the possible beam variations that the aligned beam pair $(t^{\star,\tau}, r^{\star,\tau})$ may transit to its neighbors at next channel block (as depicted in Fig. 2), a complementary set of beam pair indices is defined by $\tilde{\mathcal{C}}^{\tau+1} = \{(t^{\star,\tau}-1, r^{\star,\tau}-1), (t^{\star,\tau}-1, r^{\star,\tau}), (t^{\star,\tau}-1, r^{\star,\tau}+1), (t^{\star,\tau}, r^{\star,\tau}-1), (t^{\star,\tau}, r^{\star,\tau}+1), (t^{\star,\tau}+1, r^{\star,\tau}-1), (t^{\star,\tau}+1, r^{\star,\tau}), (t^{\star,\tau}+1, r^{\star,\tau}+1)\}$. Then, the beam training set at next channel block, i.e., $\mathcal{K}^{\tau+1}$, is given by

$$\mathcal{K}^{\tau+1} = \{\cup_t \hat{\mathcal{C}}_t^\tau\} \cup \tilde{\mathcal{C}}^{\tau+1}, \tag{17}$$

with $K^{\tau+1} \ll K^1$ $(\tau \geq 1)$ where $K^1 = |\mathcal{K}^1|$ represent the training overhead of the initial beam alignment.

Notice that the choice of α in (15) has an effect on the interpretable beam tracking performance. On the one hand, a large α is able to shrink the size of $\mathcal{C}_t^\tau$ and $\hat{\mathcal{C}}_t^\tau$, thus reducing the beam sounding overhead at next channel block. On the other hand, a shrunken $\mathcal{C}_t^\tau$ may exclude any good beam pair and cause performance deterioration. This tradeoff will be further investigated in Section V-D.

The KM learning-based beam alignment framework including training, prediction, and interpretation, is illustrated by using a toy example in Fig. 3.

IV. OPTIMIZATION METHODS FOR KM LEARNING

In this section, two new approaches to the KM learning based on DMO and dual optimization, respectively, are proposed to solve the BQP subproblem in (10), reducing the exorbitantly high computational cost of the existing SDRwR [26].

A. DISCRETE MONOTONIC OPTIMIZATION

We first present a lemma delivering an equivalent reformulation of the BQP subproblem in (10).

Lemma 1: The BQP problem in (10) is equivalent to the maximization of a difference of two monotonically increasing functions and its binary constraints $\boldsymbol{\psi}_r \in \mathbb{B}^D$ can be equivalently transformed to continuous monotonic constraints as

$$\begin{aligned} &\max_{\boldsymbol{\psi}_r} \left\{f(\boldsymbol{\psi}_r) = f^+(\boldsymbol{\psi}_r) - f^-(\boldsymbol{\psi}_r)\right\} \\ &\text{s.t. } g(\boldsymbol{\psi}_r) - h(\boldsymbol{\psi}_r) \leq 0, \boldsymbol{\psi}_r \in [\mathbf{0}, \mathbf{1}] \end{aligned} \tag{18}$$

where $f^+(\boldsymbol{\psi}_r) \triangleq 2\mathbf{v}_r^T \boldsymbol{\psi}_r$, $f^-(\boldsymbol{\psi}_r) \triangleq \boldsymbol{\psi}_r^T \mathbf{S}_r \boldsymbol{\psi}_r$, $g(\boldsymbol{\psi}_r) \triangleq \sum_{d=1}^D \psi_{r,d}$, $h(\boldsymbol{\psi}_r) \triangleq \sum_{d=1}^D \psi_{r,d}^2$, $\boldsymbol{\psi}_r \in [\mathbf{0}, \mathbf{1}]$ indicates that $0 \leq \psi_{r,d} \leq 1$ for every $d = 1, \ldots, D$, and the index of BCD iterations (υ in (10)) is omitted hereinafter for simplicity.

Proof: See Appendix B.

The combinatorial nature of the BQP problem in (10) is attributed to the discrete constraints $\boldsymbol{\psi}_r \in \mathbb{B}^D$. In [22], [26], this nuisance has been tackled by using SDRwR, which incurs impractically high computational complexity. Unlike SDRwR, the equivalent problem formulation leveraging the difference of monotonic functions (DMF) in (18) dissolves the intractable discrete constraints without any relaxation. Motivated by Lemma 1, we propose to use a branch-reduce-and-bound (BRB) algorithm [29] to directly solve (18), which consists of three main steps provided below.

1) REDUCTION

We let $M = [\mathbf{a}, \mathbf{b}]$ be one of the boxes that contain feasible solutions to (18) and ν be the current maximum value of the objective function f in (18). The reduced box $M' = [\mathbf{a}', \mathbf{b}'] \subset [\mathbf{a}, \mathbf{b}]$ can be defined by new lower and upper vertices $\mathbf{a}'$ and $\mathbf{b}'$, respectively, without excluding any feasible solution

Algorithm 2 DMO-Based Algorithm

Input: $\mathbf{S}_r$, $\mathbf{v}_r$, and D.
Output: $\boldsymbol{\psi}_r^\star$.

1: Initialization: Set iteration number $i=1$. Let $\mathcal{P}_i=\{M\}$, $M=[\mathbf{0},\mathbf{1}]$, $\mathcal{R}_i=\phi$, and $\nu=f(\mathbf{0})=0$.
2: *Reduction*: Reduce each box in $\mathcal{P}_i$ according to (19) and (20) to obtain $\mathcal{P}_i'=\{[\mathbf{a}',\mathbf{b}']|[\mathbf{a},\mathbf{b}]\in\mathcal{P}_i\}$.
3: *Bounding*: Calculate $\mu(M')$ in (21) for each $M'\in\mathcal{M}_i\triangleq\mathcal{P}_i'\cup\mathcal{R}_i$.
4: Find the feasible solution: $\boldsymbol{\psi}_r^{(i)}=\text{argmax}_{\boldsymbol{\psi}_r}\{f(\boldsymbol{\psi}_r)>\nu|\boldsymbol{\psi}_r=\lceil(\mathbf{a}'+\mathbf{b}')/2\rceil, M'=[\mathbf{a}',\mathbf{b}']\in\mathcal{M}_i\}$.
5: Update current best value: If $\boldsymbol{\psi}_r^{(i)}$ in Step 4 exists, update ν as $\nu=f(\boldsymbol{\psi}_r^{(i)})$; otherwise, $\boldsymbol{\psi}_r^{(i)}=\boldsymbol{\psi}_r^{(i-1)}$ and ν doesn't change.
6: Discarding: Delete every $M'\in\mathcal{M}_i$ such that $\mu(M')<\nu$ and let $\mathcal{R}_{i+1}$ be the collection of remaining boxes.
7: **if** $\mathcal{R}_{i+1}=\phi$ **then** terminate and **return** $\boldsymbol{\psi}_r^\star=\boldsymbol{\psi}_r^{(i)}$.
8: **else**
9: Let $M^{(i)}=\text{argmax}_{M'}\{\mu(M')|M'\in\mathcal{R}_{i+1}\}$.
10: **if** $\nu\geq\varepsilon\mu(M^{(i)})$ **then** ε-accuracy is reached and **return** $\boldsymbol{\psi}_r^\star=\boldsymbol{\psi}_r^{(i)}$.
11: **else**
12: *Branching*: Divide $M^{(i)}$ into $M_1^{(i)}$ and $M_2^{(i)}$ according to (22) and (23).
13: Update $\mathcal{R}_{i+1}$ and $\mathcal{P}_{i+1}$: $\mathcal{R}_{i+1}=\mathcal{R}_{i+1}\backslash M^{(i)}$ and $\mathcal{P}_{i+1}=\{M_1^{(i)},M_2^{(i)}\}$.
14: **end if**
15: **end if**
16: $i=i+1$ and **return** to Step 2.

$\boldsymbol{\psi}_r\in[\mathbf{a},\mathbf{b}]$, while maintaining $f(\boldsymbol{\psi}_r)\geq\nu$ [29] as

$$\mathbf{a}'=\mathbf{b}-\sum_{d=1}^{D}\alpha_d(b_d-a_d)\mathbf{e}_d, \tag{19}$$

$$\mathbf{b}'=\mathbf{a}'+\sum_{d=1}^{D}\beta_d(b_d-a_d')\mathbf{e}_d, \tag{20}$$

where $\alpha_d=\sup\{\alpha|\alpha\in[0,1], g(\mathbf{a})-h(\mathbf{b}-\alpha(b_d-a_d)\mathbf{e}_d)\leq 0, f^+(\mathbf{b}-\alpha(b_d-a_d)\mathbf{e}_d)-f^-(\mathbf{a})\geq\nu\}$ and $\beta_d=\sup\{\beta|\beta\in[0,1], g(\mathbf{a}'+\beta(b_d-a_d')\mathbf{e}_d)-h(\mathbf{b})\leq 0, f^+(\mathbf{b})-f^-(\mathbf{a}'+\beta(b_d-a_d')\mathbf{e}_d)\geq\nu\}$ for $d=1,\ldots,D$, where $\mathbf{e}_d$ is the dth column of $\mathbf{I}_D$. Note that the optimal values of α_d and β_d can be found by referring to the compactness of $\alpha,\beta\in[0,1]$ and utilizing the monotonicity of f^+, f^-, g, and h (for instance, by using a bisection method [30]).

2) BOUNDING

For every reduced box M', an upper bound of $\nu(M')\triangleq\max\{f(\boldsymbol{\psi}_r)|\ g(\boldsymbol{\psi}_r)-h(\boldsymbol{\psi}_r)\leq 0, \boldsymbol{\psi}_r\in M'\cap[\mathbf{0},\mathbf{1}]\}$ is calculated such that

$$\nu(M')\leq\mu(M')=f^+(\mathbf{b}')-f^-(\mathbf{a}'). \tag{21}$$

The upper bound $\mu(M')$ in (21) holds because f^+ and f^- are monotonically increasing functions. Furthermore, $\mu(M')$ ensures $\lim_{k\to\infty}\mu(M_k')=f(\boldsymbol{\psi}_r^\star)$, where $\{M_k'\}$ stands for any infinite nested sequence of boxes and $\boldsymbol{\psi}_r^\star$ is the optimal solution to (18). At each iteration, any box M' with $\mu(M')<\nu$ is discarded because such a box does not contain $\boldsymbol{\psi}_r^\star$ anymore.

3) BRANCHING

At the end of each iteration, the box with the maximum upper bound, denoted by $M^\star=[\mathbf{a}^\star,\mathbf{b}^\star]$, is selected and branched to accelerate the convergence of the algorithm. The box $M^\star$ is divided into two boxes

$$M_1^\star=\{\boldsymbol{\psi}_r\in M^\star|\psi_{r,j}\leq\lfloor c_j^\star\rfloor\}, \tag{22}$$

$$M_2^\star=\{\boldsymbol{\psi}_r\in M^\star|\psi_{r,j}\geq\lceil c_j^\star\rceil\}, \tag{23}$$

where $j=\text{argmax}_{d=1,\ldots,D}(b_d^\star-a_d^\star)$ and $c_j^*=(a_j^\star+b_j^\star)/2$.

The DMF optimization problem in (18) is solved by iteratively executing the above three procedures until it converges within ε-accuracy as shown in Algorithm 2. Despite the intractability of the exact complexity analysis of Algorithm 2, we can take a full-enumeration upper bound [31], i.e., 2^D, by exploiting the fact that the DMO-based method in Algorithm 2 is based on the branch-and-bound (BnB), which is close to the exhaustive search in the worst case [32]. Even though the bound 2^D is loose, it indeed provides insights into the utility of the proposed DMO-based algorithm. Algorithm 2 shows substantial efficiency when D is small (e.g., $D<10$); however, its computational cost blows up as D increases (e.g., $D>20$). This finding will be further validated in Section V-A.

B. DUAL OPTIMIZATION

An alternative approach to solving the BQP subproblem in (10) is to transform it to a dual problem. To this end, we formulate an equivalent form to the BQP in (10) as

$$\min_{\mathbf{x}\in\{+1,-1\}^D}\mathbf{x}^T\mathbf{A}_0\mathbf{x}+\mathbf{a}^T\mathbf{x}, \tag{24}$$

where ρ_r in (10) is ignored, $\mathbf{x}=2\boldsymbol{\psi}_r-\mathbf{1}\in\{+1,-1\}^D$, $\mathbf{A}_0=\frac{1}{4}\mathbf{S}_r$, and $\mathbf{a}=\frac{1}{2}\mathbf{S}_r^T\mathbf{1}-\mathbf{v}_r$. By introducing $\mathbf{X}_0=\mathbf{x}\mathbf{x}^T$ and $\mathbf{X}=\begin{bmatrix}1 & \mathbf{x}^T\\ \mathbf{x} & \mathbf{X}_0\end{bmatrix}\in\mathbb{R}^{(D+1)\times(D+1)}$, the problem in (24) can be rewritten as

$$\min_{\mathbf{x},\mathbf{X}_0}\ \langle\mathbf{X}_0,\mathbf{A}_0\rangle+\mathbf{a}^T\mathbf{x}, \tag{25a}$$

$$\text{s.t. diag}(\mathbf{X}_0)=\mathbf{1}, \tag{25b}$$

$$\mathbf{X}\succeq\mathbf{0}, \tag{25c}$$

$$\text{rank}(\mathbf{X})=1. \tag{25d}$$

Solving (25) directly is NP-hard due to the rank constraint in (25d), thus we turn to convex relaxation methods. The SDR to (25) can be expressed in a homogenized form with respect to $\mathbf{X}$ as

$$\min_{\mathbf{X}} f(\mathbf{X})\triangleq\langle\mathbf{X},\mathbf{A}\rangle, \tag{26a}$$

$$\text{s.t. }\langle\mathbf{B}_\ell,\mathbf{X}\rangle=1,\ \ell=1,\ldots,D+1, \tag{26b}$$

$$\mathbf{X} \succeq \mathbf{0}, \tag{26c}$$

where $\mathbf{A} = \begin{bmatrix} 0 & (1/2)\mathbf{a}^T \\ (1/2)\mathbf{a} & \mathbf{A}_0 \end{bmatrix} \in \mathbb{S}^{(D+1)\times(D+1)}$ and $\mathbf{B}_\ell = [\mathbf{0}_1 \ \cdots \ \mathbf{0}_{\ell-1} \ \mathbf{e}_\ell \ \mathbf{0}_{\ell+1} \ \cdots \ \mathbf{0}_{D+1}] \in \mathbb{R}^{(D+1)\times(D+1)}$. Note that the diagonal constraint in (25b) has been equivalently transformed to $D+1$ equality constraints in (26b). While the problem in (25) is combinatorial due to the rank constraint, the relaxed problem in (26) is a convex semi-definite programming (SDP). In particular, the relaxation is done by dropping the rank constraint.

We further formulate a regularized SDP formulation of (26) as

$$\begin{aligned} \min_{\mathbf{X}} \ & f_\gamma(\mathbf{X}) \triangleq \langle \mathbf{X}, \mathbf{A} \rangle + \frac{1}{2\gamma}\|\mathbf{X}\|_F^2, \\ \text{s.t.} \ & \langle \mathbf{B}_\ell, \mathbf{X} \rangle = 1, \ \ell = 1, \ldots, D+1, \\ & \mathbf{X} \succeq \mathbf{0}, \end{aligned} \tag{27}$$

where $\gamma > 0$ is a regularization parameter. With a Frobenius-norm term regularized, the strict convexity of (27) is ensured, which in turn makes strong duality hold for the feasible dual problem of (27). In this work, we leverage this fact that the duality gap is zero for (27) (a consequence of strong duality) to solve the dual problem. In addition, the two problems in (26) and (27) are equivalent as $\gamma \to \infty$.

Given the regularized SDP formulation in (27), its dual problem and the gradient of the objective function are of interest, which can be found in the following lemma.

Lemma 2: Suppose the problem in (27) is feasible. Then, the dual problem of (27) is given by

$$\max_{\mathbf{u} \in \mathbb{R}^{D+1}} \quad d_\gamma(\mathbf{u}) \triangleq -\mathbf{u}^T\mathbf{1} - \frac{\gamma}{2}\|\Pi_+(\mathbf{C}(\mathbf{u}))\|_F^2, \tag{28}$$

where $\mathbf{u} \in \mathbb{R}^{D+1}$ is the vector of Lagrange multipliers associated with each of the $D+1$ equality constraints of (27), $\mathbf{C}(\mathbf{u}) \triangleq -\mathbf{A} - \sum_{\ell=1}^{D+1} u_\ell \mathbf{B}_\ell$, and $\Pi_+(\mathbf{C}(\mathbf{u})) \triangleq \sum_{j=1}^{D+1} \max(0, \lambda_j(\mathbf{C}(\mathbf{u})))\mathbf{p}_j\mathbf{p}_j^T$, in which $\lambda_j(\mathbf{C}(\mathbf{u}))$ and $\mathbf{p}_j$, $j = 1, \ldots, D+1$, respectively, are the eigenvalue and corresponding eigenvector of $\mathbf{C}(\mathbf{u})$. The gradient of $d_\gamma(\mathbf{u})$ with respect to $\mathbf{u}$ is

$$\nabla_{\mathbf{u}} d_\gamma(\mathbf{u}) = -\mathbf{1} + \gamma\, \Phi[\Pi_+(\mathbf{C}(\mathbf{u}))], \tag{29}$$

where $\Phi[\Pi_+(\mathbf{C}(\mathbf{u}))] \triangleq [\langle \mathbf{B}_1, \Pi_+(\mathbf{C}(\mathbf{u})) \rangle, \cdots, \langle \mathbf{B}_{D+1}, \Pi_+(\mathbf{C}(\mathbf{u})) \rangle]^T \in \mathbb{R}^{D+1}$.

Proof: See Appendix C.

It is worth noting that $d_\gamma(\mathbf{u})$ in (28) is a strongly concave function, thereby making the Lagrange dual problem (28) a strongly convex problem having a unique global optimal solution [33]. Moreover, the dual problem in (28) is equivalent to the following unconstrained convex minimization problem

$$\min_{\mathbf{u} \in \mathbb{R}^{D+1}} \quad h_\gamma(\mathbf{u}) \triangleq \mathbf{u}^T\mathbf{1} + \frac{\gamma}{2}\|\Pi_+(\mathbf{C}(\mathbf{u}))\|_F^2, \tag{30}$$

with the gradient being $\nabla_{\mathbf{u}} h_\gamma(\mathbf{u}) = \mathbf{1} - \gamma\, \Phi[\Pi_+(\mathbf{C}(\mathbf{u}))]$.

An efficient, first-order method, i.e, gradient descent (GD), which is detailed in Algorithm 3, can be applied to directly solve (30). Notice that, a simple GD is proposed here owing to the fact that the dual problem in (30) is unconstrained. Indeed, we would need a projected GD method if there is any constraint involved, for which the computational complexity would be much larger (because of the projection at each iteration). In Algorithm 3, only the gradient of $h_\gamma(\mathbf{u}_i)$, i.e., $\nabla_{\mathbf{u}_i} h_\gamma(\mathbf{u}_i)$, is required to determine the descent direction. It is therefore a more practical and cost-saving method compared to standard Newton methods which demand the calculation of second-order derivatives and the inverse of the Hessian matrix. Moreover, Algorithm 3 does not rely on any approximation of the inverse of the Hessian matrix such as the quasi-Newton methods [34]. To find a step size in Step 4, we apply the backtracking line search method [35], which is based on the Armijo-Goldstein condition [36]. Finally, the algorithm is terminated when the pre-designed stopping criterion (for instance, $\|t_i\Delta\mathbf{u}_i\|_2 \le \epsilon$ in Step 5, where $\epsilon > 0$ is a predefined tolerance) is satisfied.

Algorithm 3 GD for Solving the Dual Problem in (30)

Input: $\mathbf{A}$, $\{\mathbf{B}_\ell\}_{\ell=1}^{D+1}$, D, $\mathbf{u}_0$, γ, ϵ (*tolerance threshold value*), and $I_{\max}$ (*maximum number of iterations*).
Output: $\mathbf{u}^\star$.

1: **for** $i = 0, 1, 2, \ldots, I_{\max}$ **do**
2: Calculate the gradient: $\nabla_{\mathbf{u}_i} h_\gamma(\mathbf{u}_i)$.
3: Compute the descent direction: $\Delta\mathbf{u}_i = -\nabla_{\mathbf{u}_i} h_\gamma(\mathbf{u}_i)$.
4: Find a step size t_i (via *backtracking line search*), and $\mathbf{u}_{i+1} = \mathbf{u}_i + t_i\Delta\mathbf{u}_i$.
5: **if** $\|t_i\Delta\mathbf{u}_i\|_2 \le \epsilon$ **then** terminate and **return** $\mathbf{u}^\star = \mathbf{u}_{i+1}$.
6: **end if**
7: **end for**

The solution to the dual problem in (30) (or equivalently (28)) produced by Algorithm 3, is not yet a feasible solution to the BQP in (10). A randomization procedure [37] can be employed to extract a feasible binary solution to (10) from the SDP solution $\mathbf{X}^\star$ of (27). One typical design of the randomization procedure for BQP is to generate feasible points from the Gaussian random samples via rounding [38]. The Gaussian randomization procedure provides a tight approximation with probability $1 - \exp(-\mathcal{O}(D))$, asymptotically in D [39]. By leveraging the fact that the eigenvalues and corresponding eigenvectors of $\Pi_+(\mathbf{C}(\mathbf{u}))$ can be found by Step 2 of Algorithm 3, we have

$$\mathbf{X}^\star = \gamma\,\Pi_+(\mathbf{C}(\mathbf{u}^\star)) = \gamma\mathbf{V}_+\Lambda_+\mathbf{V}_+^T = \mathbf{L}\mathbf{L}^T,$$

where $\Pi_+(\mathbf{C}(\mathbf{u})) \triangleq \mathbf{V}_+\Lambda_+\mathbf{V}_+^T$ and $\mathbf{L} = \mathbf{V}_+\sqrt{\gamma\Lambda_+}$. A detailed randomization procedure is provided in Algorithm 4.

In Step 8 of Algorithm 4, the D-dimensional vector $\hat{\mathbf{x}}$ is first recovered from a $(D+1)$-dimensional vector $\tilde{\mathbf{x}}_{\ell^\star}$ by considering the structure of $\mathbf{X}$ in (25), and then used to approximate the BQP solution based on (24). Also note that the randomization performance improves with I_{rand}. In practice, we only need to choose a sufficient but not excessive I_{rand} (for instance, $50 \le I_{\text{rand}} \le 100$) achieving a good approximation

Algorithm 4 Randomization

Input: $\mathbf{A}$, $\Pi_+(\mathbf{C}(\mathbf{u}^\star)) = \mathbf{V}_+\Lambda_+\mathbf{V}_+^T$, D, γ, and I_{rand} (*the number of randomizations*).
Output: $\hat{\boldsymbol{\psi}}$ (an approximate solution to the BQP in (10)).
1: Obtain $\mathbf{L} = \mathbf{V}_+\sqrt{\gamma\Lambda_+}$ and $\mathbf{L}\mathbf{L}^T = \mathbf{X}^\star$.
2: **for** $l = 1, 2, \ldots, I_{\text{rand}}$ **do**
3: Generation of an i.i.d. Gaussian random vector: $\boldsymbol{\xi}_l \sim \mathcal{N}(\mathbf{0}, \mathbf{I}_{D+1})$.
4: Random sampling: $\tilde{\boldsymbol{\xi}}_l = \mathbf{L}\boldsymbol{\xi}_l$.
5: Discretization: $\tilde{\mathbf{x}}_l = \text{sign}(\tilde{\boldsymbol{\xi}}_l)$.
6: **end for**
7: Determine $l^\star = \text{argmin}_{l=1,\ldots,I_{\text{rand}}} \tilde{\mathbf{x}}_l^T\mathbf{A}\tilde{\mathbf{x}}_l$.
8: Approximation: $\hat{\mathbf{x}} = \tilde{x}_{l^\star,1}\cdot\tilde{\mathbf{x}}_{l^\star,2:D+1}$ and $\hat{\boldsymbol{\psi}} = \frac{\hat{\mathbf{x}}_{+\mathbf{1}}}{2}$.

for the BQP solution. Moreover, its overall computational complexity is much smaller than the conventional randomization algorithms [26], [37], [38] because our proposed Algorithm 4 does not require the computation of the Cholesky factorization. Finally, the computational complexity of the dual optimization with GD (i.e., "Dual+GD") is dominated by the EVD of a $(D+1)\times(D+1)$ matrix, needed to compute $\nabla_{\mathbf{u}_i} h_\gamma(\mathbf{u}_i)$ in Step 2 of Algorithm 3, which is given by $\mathcal{O}((D+1)^3)$. This is indeed a significant improvement compared to the existing SDRwR with complexity $\mathcal{O}(D^{4.5})$ [26], especially when D is large.

V. NUMERICAL RESULTS

In this section, we perform numerical evaluations of the proposed KM learning methods for beam alignment/tracking by incorporating the predictability and interpretability. In the experiments, a beam space MIMO channel representation of sparse mmWave channels is adopted [13], [14], [40] and the rank of channel matrix is assumed to be 1. In particular, the channel $\mathbf{H}$ in (3) is represented by

$$\mathbf{H} = \mathbf{D}_r\mathbf{H}_v\mathbf{D}_t^*,$$

where $\mathbf{D}_r \in \mathbb{C}^{N_r\times N_r}$ and $\mathbf{D}_t \in \mathbb{C}^{N_t\times N_t}$ are unitary discrete Fourier transform matrices, while $\mathbf{H}_v \in \mathbb{C}^{N_r\times N_t}$ denotes the virtual channel matrix of $\mathbf{H}$. Let $H_v^\tau \in \mathbb{C}$ be the nonzero entry of $\mathbf{H}_v^\tau$ and $L(H_v^\tau)$ be the associated support location (extracting the row-column information of H_v^τ) at τth channel block. The temporal correlation between channel realizations (from channel block τ to $\tau+1$) is modeled by considering the following two parts: i) Channel coefficient evolution. The evolution of the propagation path gain can be modeled via the first-order Gauss-Markov process [41]–[43] as

$$H_v^{\tau+1} = \rho H_v^\tau + \sqrt{1-\rho^2}v^{\tau+1}, \tag{31}$$

where $\rho \in [0, 1]$ is the temporal correlation coefficient and $v^{\tau+1} \sim \mathcal{CN}(0, 1)$ denotes the innovation process independent of H_v^τ. The adoption of the Gauss-Markov process in the spatial channel model [44], which is officially used in 3GPP LTE [45], has been established in [42]. ii) Support/beam variation. The slow variation of the support in $\mathbf{H}_v^\tau$ is modeled by assuming that the support can only switch to its neighbors and introducing a support transition probability defined as

$$p \triangleq \Pr(L(H_v^{\tau+1}) \in \mathcal{L}^{\tau+1} | L(H_v^\tau) \in \mathcal{L}^\tau) \in [0, 1], \tag{32}$$

where $\mathcal{L}^\tau = \{(i, j)\}$ returns the original location (ith row and jth column of $\mathbf{H}_v^\tau$) of the support at τth channel block and $\mathcal{L}^{\tau+1} = \{(i-1, j-1), (i-1, j), (i-1, j+1), (i, j-1), (i, j+1), (i+1, j-1), (i+1, j), (i+1, j+1)\}$ is the set composed of all possible support transition locations at $(\tau+1)$th channel block. Note that under the assumption of temporal correlation, past CSI can be reused to refine the quality of the current beam alignment and reduce the beam tracking overhead. This can be achieved by exploiting the interpretability of KM as demonstrated in Section III-B.

Moreover, we set $N_t = N_r = |\mathcal{I}_\mathcal{F}| = |\mathcal{I}_\mathcal{W}|$, $I_{\text{BCD}} = 10$, $I_{\text{rand}} = 100$, and $T_{\text{FE}} = 8$ throughout the simulations. We evaluate the performance from the following four different perspectives. In particular, we focus on the initial beam alignment ($\tau = 1$) from Section V-A to Section V-C, while the beam tracking ($\tau > 1$) is considered in Section V-D.

A. COMPUTATIONAL COST

We first compare the computational cost of the two proposed KM learning methods (including the KM with DMO in Algorithm 2 and Dual+GD in Algorithm 3) with the existing KM learning with SDRwR in [22, Algorithm 1]. The computational cost is evaluated by averaging the total running time in seconds (measured by "cputime" in MATLAB running on a PC with an Intel Xeon E5-1650 v3 3.50 GHz CPU and 32 GB RAM) over 100 Monte Carlo simulations. Note that the sampling rate for the initial beam alignment, defined as the ratio of the number of beam pairs in the subsampled training set at $\tau = 1$ to the total number of the beam pairs in the original codebook, is given by SR $= |\mathcal{K}|/|\mathcal{S}|$ (the superscript '$\tau = 1$' of $\mathcal{K}$ is omitted for brevity).

Table 1 lists the time consumption (in seconds) of the overall KM learning with three different algorithms for varying D, N_t, N_r, and SR. It can be seen that the proposed methods can achieve a reduced computational cost up to three orders of magnitude, compared with the existing KM learning with SDRwR. Especially, the KM with DMO shows benefits when D is small while the KM with Dual+GD exhibits better performance when D is large. The above numerical results coincide with the theoretical analyses in Section IV.

B. TRAINING AND PREDICTION PERFORMANCE

The training and prediction performance of the proposed methods is assessed by adopting the root-mean-square-error (RMSE) as a metric. The RMSEs for the training and prediction phases, respectively, are given by

$$E_{\text{train}} \triangleq \left(\frac{1}{|\mathcal{K}|}\sum_{(t,r)\in\mathcal{K}} |p_{t,r} - \boldsymbol{\theta}_t^{\star T}\boldsymbol{\psi}_r^\star|^2\right)^{\frac{1}{2}},$$

$$E_{\text{test}} \triangleq \left(\frac{1}{|\mathcal{T}|}\sum_{(t,r)\in\mathcal{T}} |p_{t,r} - \boldsymbol{\theta}_t^{\star T}\boldsymbol{\psi}_r^\star|^2\right)^{\frac{1}{2}}.$$

TABLE 1. Time consumption (in seconds) comparison of the KM learning-based methods.

SR	Algorithms	$N_t = N_r = 16$			$N_t = N_r = 64$		
		$D = 4$	$D = 8$	$D = 16$	$D = 4$	$D = 8$	$D = 16$
50%	KM with SDRwR	2.23×10^3	2.37×10^3	2.52×10^3	8.57×10^3	9.02×10^3	9.79×10^3
	KM with DMO	1.36	1.92	4.02×10^2	1.05×10^1	1.17×10^1	6.10×10^2
	KM with Dual+GD	1.08×10^1	1.96×10^1	3.15×10^1	5.03×10^1	1.34×10^2	2.85×10^2
25%	KM with SDRwR	2.04×10^3	2.15×10^3	2.31×10^3	8.01×10^3	8.49×10^3	9.10×10^3
	KM with DMO	1.17	1.38	9.56×10^1	6.53	8.22	3.75×10^2
	KM with Dual+GD	7.99	1.33×10^1	2.96×10^1	4.10×10^1	8.78×10^1	1.16×10^2

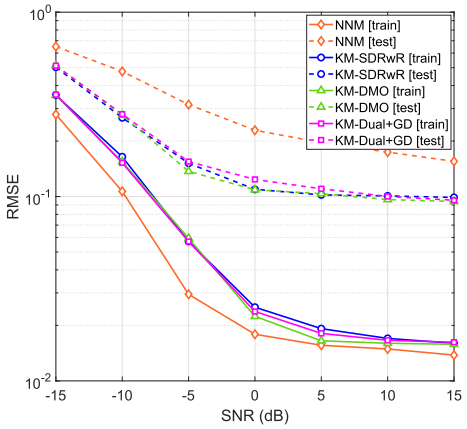

FIGURE 4. The training and prediction performance comparison when $N_t = N_r = 16$, $D = 8$, $\delta = 12$ dB, and SR = 25%.

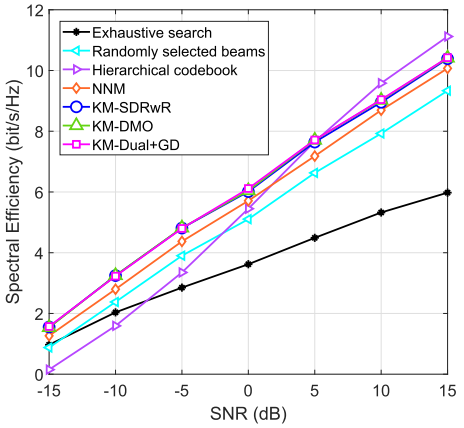

FIGURE 5. The effective spectral efficiency comparison for the initial beam alignment ($\tau = 1$) when $N_t = N_r = 16$, $D = 8$, and $\delta = 12$ dB.

Fig. 4 displays the train and test RMSEs of the proposed KM learning methods and the existing KM learning with SDRwR, as a function of SNR, for $N_t = N_r = 16$, $D = 8$, $\delta = 16$ dB, and SR = 25%. Besides, another learning-based technique called the nonnegative model (NNM) [46], which is a convex relaxation of the KM, is included as a benchmark. While the NNM has a similar structure as the KM in (2), the difference is that the NNM relaxes the binary constraints on $\boldsymbol{\psi}_r$ to a nonnegative box, i.e., $\boldsymbol{\psi}_r \in [\mathbf{0}, \mathbf{1}]$. It can be observed that the proposed methods can achieve similar good training and prediction performance as the existing KM learning with SNRwR by using only a quarter of samples, while reducing the computational cost substantially as shown in Table 1. Despite a slightly better training performance of the NNM, its prediction counterpart is significantly deteriorated compared to the KM learning-based methods due to the fact that $\boldsymbol{\theta}_u^T \boldsymbol{\psi}_r$ with a relaxed indicator vector $\boldsymbol{\psi}_r$ of NNM no longer represents the outcome of a random variable. This further leads to a degradation of the beam alignment performance, which can be found in Section V-C.

C. SPECTRAL EFFICIENCY

Next, we evaluate the performance of the proposed approaches regarding the predictive beam alignment for the initial channel block ($\tau = 1$). Several conventional beam alignment techniques including the exhaustive beam search, randomly selected beams, and hierarchical codebook, are considered as the baselines. For a fair comparison, we adopt the effective spectral efficiency as a metric, which is defined as

$$R = \frac{T-K}{T} \log_2(1+\eta),$$

where the pre-log factor $(T-K)/T$ represents the portion of channel coherent resources contributed to data communication. In particular, the sampling rate for the exhaustive search and randomly selected beams is 100% and 25%, respectively. By taking account of both the training overhead ($2\log_2 N_t + 2\log_2 N_r$) and feedback overhead ($\log_2 N_t$), the sampling rate for the hierarchical codebook is 8% [7]. We set the sampling rate for the KM learning-based methods and NNM to be SR= 25%.

In Fig. 5, we plot the effective spectral efficiency versus SNR by considering the initial beam alignment for $N_t = N_r = 16$, $D = 8$, $\delta = 12$ dB, and assuming that the channel block length is $T = 512$ channel uses. It can be found that our proposed methods outperform the exhaustive search, randomly selected beams and NNM throughout the entire SNR region. In addition, despite a slightly better performance shown by the hierarchical codebook when the SNR is high, a superior performance in the low SNR regime of the proposed methods can be observed, which is more appreciated in mmWave communication systems.

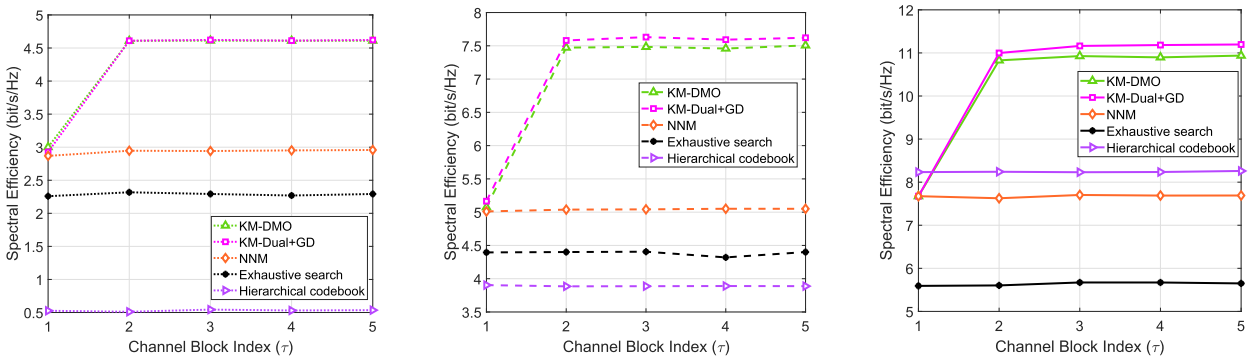

FIGURE 6. The interpretable beam tracking performance comparison when $N_t = N_r = 16$, $D = 8$, $\delta = 12$ dB, $p = 0.05$, $\rho = 0.95$, and $\alpha = 0.75$: (a) SNR= -10 dB, (b) SNR= 0 dB, (c) SNR= 10 dB.

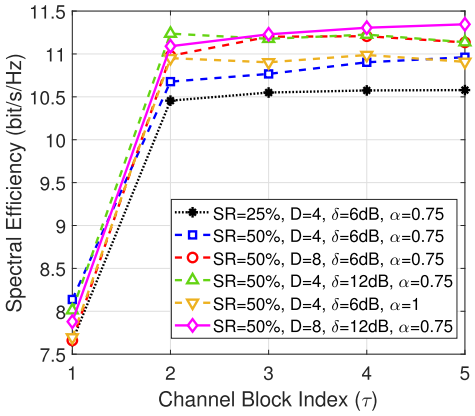

FIGURE 7. The effect of parameter settings on beam tracking performance of KM learning with Dual+GD when $N_t = N_r = 16$, $p = 0.05$, $\rho = 0.95$, and SNR= 10 dB.

D. LOW-LATENCY BEAM TRACKING VIA INTERPRETABILITY

Finally, the interpretable beam tracking performance is evaluated by considering multiple channel blocks ($\tau = 1, \ldots, 5$). The temporal correlation coefficient parameter ρ in (31) and the support transition probability p in (32) are set to 0.95 and 0.05, respectively. In Fig. 6, we depict the effective spectral efficiency with a variation of the channel block index for $N_t = N_r = 16$, $D = 8$, $\delta = 12$ dB, and $\alpha = 0.75$ under three different scenarios of SNR. For the initial beam alignment when $\tau = 1$, we assume SR = 50% for the proposed KM learning-based methods and NNM. It can be seen that, by exploiting the interpretability of KM, the proposed methods can be well adapted to the channel temporal correlation and beam variation, and subsequently exhibit significantly better performance than the baseline schemes in term of beam tracking. In particular, due to the relaxation of the binary indicator vector $\boldsymbol{\psi}_r$, the NNM sacrifices the highly interpretable nature of KM. Moreover, the KM with Dual+GD shows a slightly better performance than the KM with DMO when the SNR is high, while the two proposed KM learning methods perform indistinguishably in the low SNR regime.

We further investigate the impact of different parameter settings on the beam tracking performance of the proposed KM learning with Dual+GD when $N_t = N_r = 16$, $p = 0.05$, $\rho = 0.95$, and SNR= 10 dB. It is observed from Fig. 7 that the effective spectral efficiency improves with the increase of SR. This is attributed to the fact that the accuracy of the initial beam alignment plays an essential role in succeeding beam tracking. Besides, a performance improvement can be attained as D and δ grow. By increasing α in (15), the spectral efficiency increases a lot at the beginning, but degrades as the channel block index grows. This phenomenon can be interpreted as: the performance improvement is due to the significantly reduced beam tracking overhead as α increases, while a high α excludes potential beam pairs which further leads to the performance degradation in subsequent channel blocks.

VI. CONCLUSION

In this paper, we investigated a joint scheme of predictive beam alignment and interpretable beam tracking for mmWave communication systems. The distinctive and powerful interpretability of KM has been exploited to achieve an agile beam tracking with low latency. Moreover, two enhanced KM learning algorithms were proposed, by leveraging DMO and dual optimization, to reduce the computational cost of the existing KM learning with SDRwR by up to three orders of magnitude. Numerical results demonstrated the superiority of the proposed KM learning methods compared to other benchmarks in terms of computational complexity, training/prediction performance, spectral efficiency for beam alignment/tracking, and robustness in the low SNR regime.

APPENDIX A
PROOF OF THEOREM 1

The two random variables X_{t,r_1} and X_{t,r_2} share the same alphabet $\mathcal{X} = \{1, 0\}$. By (1), $X_{t,r_1}^{-1}(\{\mathcal{X}(x)\})$ and $X_{t,r_2}^{-1}(\{\mathcal{X}(x)\})$ represent the inverse images of the events $X_{t,r_1} = \mathcal{X}(x)$ and $X_{t,r_2} = \mathcal{X}(x)$, $x \in \{1, 2\}$, respectively. According to (2), we have $\psi_{r,d} = 1$ only if $\omega_d \in X_{t,r}^{-1}(\{\mathcal{X}(1)\})$, $r \in \{r_1, r_2\}$, $d \in \{1, \ldots, D\}$. Therefore, we obtain that $\text{supp}(\boldsymbol{\psi}_{r_2}) \subseteq$

$\text{supp}(\boldsymbol{\psi}_{r_1}) \Rightarrow X_{t,r_2}^{-1}(\{\mathcal{X}(1)\}) \subseteq X_{t,r_1}^{-1}(\{\mathcal{X}(1)\})$, and consequently $X_{t,r_1}=1 \Rightarrow X_{t,r_2}=1$ ($\gamma_{t,r_1} \geq \delta \Rightarrow \gamma_{t,r_2} \geq \delta$).

Moreover, the fact that $\Omega = X_{t,r}^{-1}(\{\mathcal{X}(1)\}) \cup X_{t,r}^{-1}(\{\mathcal{X}(2)\})$ and $X_{t,r}^{-1}(\{\mathcal{X}(1)\}) \cap X_{t,r}^{-1}(\{\mathcal{X}(2)\}) = \phi$, $r \in \{r_1, r_2\}$, results in $\text{supp}(\boldsymbol{\psi}_{r_2}) \subseteq \text{supp}(\boldsymbol{\psi}_{r_1}) \Rightarrow X_{t,r_1}^{-1}(\{\mathcal{X}(2)\}) \subseteq X_{t,r_2}^{-1}(\{\mathcal{X}(2)\})$, which further leads to $X_{t,r_2}=0 \Rightarrow X_{t,r_1}=0$ ($\gamma_{t,r_2} < \delta \Rightarrow \gamma_{t,r_1} < \delta$).

APPENDIX B
PROOF OF LEMMA 1

Given the definition of f^+ and f^- in (18), the objective function f in (18) is attained by transforming the minimization to the maximization and discarding the constant ρ_r in (10). Besides, f^+ and f^- are both increasing functions with respect to $\boldsymbol{\psi}_r \in [\mathbf{0}, \mathbf{1}]$ because $\mathbf{v}_r > \mathbf{0}$ and $\mathbf{S}_r$ is PSD.

The binary constraints $\psi_{r,d} \in \{0, 1\}, d = 1, \ldots, D$, can be equivalently rewritten as

$$\sum_{d=1}^{D} \psi_{r,d}(1-\psi_{r,d}) \leq 0, \ \psi_{r,d} \in [0, 1], \ \forall d \in \{1, \ldots, D\},$$

which is exactly $g(\boldsymbol{\psi}_r)-h(\boldsymbol{\psi}_r) \leq 0$, $\boldsymbol{\psi}_r \in [\mathbf{0}, \mathbf{1}]$ in (18), where g and h are increasing on $\mathbb{R}_+^D$.

APPENDIX C
PROOF OF LEMMA 2

The Lagrangian of the primal problem in (27) is given by

$$\begin{aligned}&\mathcal{L}(\mathbf{X}, \mathbf{u}, \mathbf{D})\\ &\text{e}= \langle \mathbf{X}, \mathbf{A}\rangle + \frac{1}{2\gamma}\|\mathbf{X}\|_F^2 - \langle \mathbf{X}, \mathbf{D}\rangle + \sum_{\ell=1}^{D+1} u_\ell(\langle \mathbf{X}, \mathbf{B}_\ell\rangle - 1), \quad (33)\end{aligned}$$

where $\mathbf{u} \in \mathbb{R}^{D+1}$ and $\mathbf{D} \succeq \mathbf{0}$ are Lagrangian multipliers. Since the problems in (27) and (33) are feasible, strong duality holds and $\nabla_{\mathbf{X}}\mathcal{L}(\mathbf{X}^\star, \mathbf{u}^\star, \mathbf{D}^\star) = 0$, where $\mathbf{X}^\star$, $\mathbf{u}^\star$, and $\mathbf{D}^\star$ are optimal solutions to (33). Then we have

$$\mathbf{X}^\star = \gamma\left(\mathbf{D}^\star - \mathbf{A} - \sum_{\ell=1}^{D+1} u_\ell^\star \mathbf{B}_\ell\right) = \gamma(\mathbf{D}^\star + \mathbf{C}(\mathbf{u}^\star)), \quad (34)$$

where $\mathbf{C}(\mathbf{u}^\star) = -\mathbf{A} - \sum_{\ell=1}^{D+1} u_\ell^\star \mathbf{B}_\ell$. Substituting $\mathbf{X}^\star$ in (33), we obtain the dual formulation

$$\max_{\mathbf{u}\in\mathbb{R}^{D+1}, \mathbf{D}\succeq\mathbf{0}} \ -\mathbf{u}^T\mathbf{1} - \frac{\gamma}{2}\|\mathbf{D}+\mathbf{C}(\mathbf{u})\|_F^2. \quad (35)$$

For a given $\mathbf{u}$, the dual problem in (35) is equivalent to

$$\min_{\mathbf{D}\succeq\mathbf{0}} \ \frac{\gamma}{2}\|\mathbf{D}+\mathbf{C}(\mathbf{u})\|_F^2. \quad (36)$$

The solution to (36) is $\mathbf{D}^\star = \Pi_+(-\mathbf{C}(\mathbf{u}))$. Due to the fact that $\mathbf{C}(\mathbf{u}) = \Pi_+(\mathbf{C}(\mathbf{u})) - \Pi_+(-\mathbf{C}(\mathbf{u}))$, it follows $\mathbf{D}^\star + \mathbf{C}(\mathbf{u}) = \Pi_+(\mathbf{C}(\mathbf{u}))$. Thus the dual formulation in (35) can be simplified to (28).

We take the first-order derivative of $d_\gamma(\mathbf{u})$ in (28) with respect to $\mathbf{u}$ and obtain

$$\begin{aligned}\nabla_{\mathbf{u}} d_\gamma(\mathbf{u}) &= -\mathbf{1} - \gamma\nabla_{\mathbf{u}}\left(\frac{1}{2}\|\Pi_+(\mathbf{C}(\mathbf{u}))\|_F^2\right)\\ &= -\mathbf{1} + \gamma\,\Phi[\Pi_+(\mathbf{C}(\mathbf{u}))],\end{aligned}$$

where the last equality is due to $\nabla_{\mathbf{Z}}(\frac{1}{2}\|\Pi_+(\mathbf{Z})\|_F^2) = \nabla_{\mathbf{Z}}(\frac{1}{2}\sum_{i=1}^{N}(\max(0, \lambda_i(\mathbf{Z})))^2) = \Pi_+(\mathbf{Z})$, where $\lambda_i(\mathbf{Z})$ is the ith eigenvalue of $\mathbf{Z} \in \mathbb{R}^{N\times N}$.

REFERENCES

[1] S. Hur, T. Kim, D. J. Love, J. V. Krogmeier, T. A. Thomas, and A. Ghosh, "Millimeter wave beamforming for wireless backhaul and access in small cell networks," *IEEE Trans. Commun.*, vol. 61, no. 10, pp. 4391–4403, Oct. 2013.

[2] R. W. Heath, Jr., N. González-Prelcic, S. Rangan, W. Roh, and A. M. Sayeed, "An overview of signal processing techniques for millimeter wave MIMO systems," *IEEE J. Sel. Topics Signal Process.*, vol. 10, no. 3, pp. 436–453, Apr. 2016.

[3] *Study on New Radio Access Technology Physical Layer Aspects-Release 14*, document TR 38.802, 3GPP, Technical Specification Group Radio Access Network, Mar. 2017.

[4] W. Roh, J.-Y. Seol, J. Park, B. Lee, J. Lee, Y. Kim, J. Cho, K. Cheun, and F. Aryanfar, "Millimeter-wave beamforming as an enabling technology for 5G cellular communications: Theoretical feasibility and prototype results," *IEEE Commun. Mag.*, vol. 52, no. 2, pp. 106–113, Feb. 2014.

[5] J. Zhang, X. Ge, Q. Li, M. Guizani, and Y. Zhang, "5G millimeter-wave antenna array: Design and challenges," *IEEE Wireless Commun.*, vol. 24, no. 2, pp. 106–112, Apr. 2017.

[6] A. Alkhateeb, O. El Ayach, G. Leus, and R. W. Heath, Jr., "Channel estimation and hybrid precoding for millimeter wave cellular systems," *IEEE J. Sel. Topics Signal Process.*, vol. 8, no. 5, pp. 831–846, Oct. 2014.

[7] Z. Xiao, T. He, P. Xia, and X.-G. Xia, "Hierarchical codebook design for beamforming training in millimeter-wave communication," *IEEE Trans. Wireless Commun.*, vol. 15, no. 5, pp. 3380–3392, May 2016.

[8] Y. M. Tsang, A. S. Y. Poon, and S. Addepalli, "Coding the beams: Improving beamforming training in mmWave communication system," in *Proc. IEEE Global Telecommun. Conf. (GLOBECOM)*, Dec. 2011, pp. 1–6.

[9] Y. Shabara, C. E. Koksal, and E. Ekici, "Beam discovery using linear block codes for millimeter wave communication networks," *IEEE/ACM Trans. Netw.*, vol. 27, no. 4, pp. 1446–1459, Aug. 2019.

[10] M. Kokshoorn, H. Chen, P. Wang, Y. Li, and B. Vucetic, "Millimeter wave MIMO channel estimation using overlapped beam patterns and rate adaptation," *IEEE Trans. Signal Process.*, vol. 65, no. 3, pp. 601–616, Feb. 2017.

[11] H. Hassanieh, O. Abari, M. Rodreguez, M. Abdelghany, D. Katabi, and P. Indyk, "Agile millimeter wave networks with provable guarantees," *CoRR*, vol. abs/1706.06935, pp. 1–14, Jun. 2017.

[12] A. J. Duly, T. Kim, D. J. Love, and J. V. Krogmeier, "Closed-loop beam alignment for massive MIMO channel estimation," *IEEE Commun. Lett.*, vol. 18, no. 8, pp. 1439–1442, Aug. 2014.

[13] T. Kim and D. J. Love, "Virtual AoA and AoD estimation for sparse millimeter wave MIMO channels," in *Proc. IEEE 16th Int. Workshop Signal Process. Adv. Wireless Commun. (SPAWC)*, Jun. 2015, pp. 146–150.

[14] Q. Duan, T. Kim, H. Huang, K. Liu, and G. Wang, "AoD and AoA tracking with directional sounding beam design for millimeter wave MIMO systems," in *Proc. IEEE 26th Annu. Int. Symp. Pers., Indoor, Mobile Radio Commun. (PIMRC)*, Aug. 2015, pp. 2271–2276.

[15] H. Ghauch, T. Kim, M. Bengtsson, and M. Skoglund, "Subspace estimation and decomposition for large millimeter-wave MIMO systems," *IEEE J. Sel. Topics Signal Process.*, vol. 10, no. 3, pp. 528–542, Apr. 2016.

[16] S. Sun and T. S. Rappaport, "Millimeter wave MIMO channel estimation based on adaptive compressed sensing," in *Proc. IEEE Int. Conf. Commun. Workshops (ICC Workshops)*, May 2017, pp. 47–53.

[17] W. Zhang, T. Kim, D. J. Love, and E. Perrins, "Leveraging the restricted isometry property: Improved low-rank subspace decomposition for hybrid millimeter-wave systems," *IEEE Trans. Commun.*, vol. 66, no. 11, pp. 5814–5827, Nov. 2018.

[18] M. Xiao, S. Mumtaz, Y. Huang, L. Dai, Y. Li, M. Matthaiou, G. K. Karagiannidis, E. Björnson, K. Yang, C.-L. I, and A. Ghosh, "Millimeter wave communications for future mobile networks," *IEEE J. Sel. Areas Commun.*, vol. 35, no. 9, pp. 1909–1935, Sep. 2017.

[19] M. Giordani, M. Polese, A. Roy, D. Castor, and M. Zorzi, "A tutorial on beam management for 3GPP NR at mmWave frequencies," *IEEE Commun. Surveys Tuts.*, vol. 21, no. 1, pp. 173–196, 1st Quart., 2019.

[20] L. You, X. Chen, X. Song, F. Jiang, W. Wang, X. Gao, and G. Fettweis, "Network massive MIMO transmission over millimeter-wave and terahertz bands: Mobility enhancement and blockage mitigation," *IEEE J. Sel. Areas Commun.*, vol. 38, no. 12, pp. 2946–2960, Dec. 2020.
[21] M. Hussain, M. Scalabrin, M. Rossi, and N. Michelusi, "Mobility and blockage-aware communications in millimeter-wave vehicular networks," *IEEE Trans. Veh. Technol.*, vol. 69, no. 11, pp. 13072–13086, Nov. 2020.
[22] W. M. Chan, H. Ghauch, T. Kim, E. De Carvalho, and G. Fodor, "Kolmogorov model for large millimeter-wave antenna arrays: Learning-based beam-alignment," in *Proc. 53rd Asilomar Conf. Signals, Syst., Comput.*, Nov. 2019, pp. 411–415.
[23] Q. Duan, T. Kim, H. Ghauch, and E. W. M. Wong, "Enhanced beam alignment for millimeter wave MIMO systems: A Kolmogorov model," in *Proc. IEEE Global Commun. Conf. (GLOBECOM)*, Dec. 2020, pp. 1–6.
[24] M. Jaggi, "Revisiting Frank–Wolfe: Projection-free sparse convex optimization," in *Proc. 30th Int. Conf. Mach. Learn.*, 2013, vol. 28, no. 1, pp. 427–435.
[25] M. Kisialiou and Z.-Q. Luo, "Probabilistic analysis of semidefinite relaxation for binary quadratic minimization," *SIAM J. Optim.*, vol. 20, no. 4, pp. 1906–1922, Jan. 2010.
[26] H. Ghauch, M. Skoglund, H. Shokri-Ghadikolaei, C. Fischione, and A. H. Sayed, "Learning Kolmogorov models for binary random variables," in *Proc. ICML Workshop Non-Convex Optim.*, 2018, pp. 1–9.
[27] R. M. Gray, *Probability, Random Process, and Ergodic Properties*. New York, NY, USA: Springer, 2009.
[28] A. N. Kolmogorov, "On the representation of continuous functions of many variables by superposition of continuous functions of one variable and addition," *Doklady Akademii Nauk SSSR*, vol. 114, no. 5, pp. 953–956, 1957.
[29] H. Tuy, M. Minoux, and N. T. Hoai-Phuong, "Discrete monotonic optimization with application to a discrete location problem," *SIAM J. Optim.*, vol. 17, no. 1, pp. 78–97, Jan. 2006.
[30] T. Kim, D. J. Love, M. Skoglund, and Z.-Y. Jin, "An approach to sensor network throughput enhancement by PHY-aided MAC," *IEEE Trans. Wireless Commun.*, vol. 14, no. 2, pp. 670–684, Feb. 2015.
[31] T. Denat, A. Harutyunyan, and V. T. Paschos, "Average-case complexity of a branch-and-bound algorithm for min dominating set," *CoRR*, vol. abs/1902.01874, pp. 1–7, Feb. 2019.
[32] H. Tuy, F. Al-Khayyal, and P. T. Thach, *Monotonic Optimization: Branch and Cut Methods*. Boston, MA, USA: Springer, 2005, pp. 39–78.
[33] S. Boyd and L. Vandenberghe, *Convex Optimization*. Cambridge, U.K.: Cambridge Univ. Press, 2004.
[34] P. Wang, C. Shen, A. V. D. Hengel, and P. H. S. Torr, "Large-scale binary quadratic optimization using semidefinite relaxation and applications," *IEEE Trans. Pattern Anal. Mach. Intell.*, vol. 39, no. 3, pp. 470–485, Mar. 2017.
[35] D. P. Bertsekas, *Nonlinear Programming*, 3rd ed. Belmont, MA, USA: Athena Scientific, 2016.
[36] L. Armijo, "Minimization of functions having Lipschitz continuous first partial derivatives," *Pacific J. Math.*, vol. 16, no. 1, pp. 1–3, 1966.
[37] M. X. Goemans and D. P. Williamson, "Improved approximation algorithms for maximum cut and satisfiability problems using semidefinite programming," *J. Assoc. Comput. Mach.*, vol. 42, no. 6, pp. 1115–1145, Nov. 1995.
[38] Z.-Q. Luo, W.-K. Ma, A. M.-C. So, Y. Ye, and S. Zhang, "Semidefinite relaxation of quadratic optimization problems," *IEEE Signal Process. Mag.*, vol. 27, no. 3, pp. 20–34, May 2010.
[39] M. Kisialiou and Z.-Q. Luo, "Performance analysis of quasi-maximum-likelihood detector based on semi-definite programming," in *Proc. IEEE Int. Conf. Acoust., Speech, Signal Process. (ICASSP)*, vol. 3, Mar. 2005, pp. 433–436.
[40] A. M. Sayeed, "Deconstructing multiantenna fading channels," *IEEE Trans. Signal Process.*, vol. 50, no. 10, pp. 2563–2579, Oct. 2002.
[41] R. H. Etkin and D. N. C. Tse, "Degrees of freedom in some underspread MIMO fading channels," *IEEE Trans. Inf. Theory*, vol. 52, no. 4, pp. 1576–1608, Apr. 2006.
[42] T. Kim, D. J. Love, and B. Clerckx, "MIMO systems with limited rate differential feedback in slowly varying channels," *IEEE Trans. Commun.*, vol. 59, no. 4, pp. 1175–1189, Apr. 2011.
[43] T. Kim, D. J. Love, and B. Clerckx, "Does frequent low resolution feedback outperform infrequent high resolution feedback for multiple antenna beamforming systems?" *IEEE Trans. Signal Process.*, vol. 59, no. 4, pp. 1654–1669, Apr. 2011.
[44] J. Salo, G. D. Galdo, J. Salmi, P. Kyosti, M. Milojevic, D. Laselva, and C. Schneider, *MATLAB Implementation of the 3GPP Spatial Channel Model*, document TR 25.996, 3GPP, 2005.
[45] *3GPP LTE: Evolved Packet System RAN Part-Release 8*, document TS 22.278, 3GPP, LTE, Dec. 2009.
[46] C. J. Stark, "Expressive recommender systems through normalized nonnegative models," in *Proc. 30th AAAI Conf. Artif. Intell.*, 2016, pp. 1081–1087.

QIYOU DUAN received the B.Eng. degree (Hons.) in electrical engineering and the B.Sc. degree in finance from Wuhan University, Wuhan, China, in 2014. He is currently pursuing the Ph.D. degree with the Department of Electrical Engineering, City University of Hong Kong, Hong Kong. From January 2018 to July 2018, he was a Visiting Scholar with the Department of Electrical Engineering and Computer Science, The University of Kansas, Lawrence, KS, USA. His research interests include signal processing, millimeter-wave communications, optimization methods, and machine learning.

TAEJOON KIM (Senior Member, IEEE) received the Ph.D. degree in electrical and computer engineering from Purdue University, West Lafayette, IN, USA, in 2011.

He was with Nokia Bell Labs, Berkeley, CA, USA, as a Senior Researcher. Prior to joining the University of Kansas (KU) as an Assistant Professor, he was a Postdoctoral Researcher at KTH, Stockholm, Sweden, and an Assistant Professor at the City University of Hong Kong. He holds 29 issued U.S. patents. His research interests include 5G-and-beyond wireless systems, multiple-input multiple-output (MIMO) communications, millimeter wave and terahertz wireless, statistical inference, array signal processing, and machine learning. He was a recipient of Miller Faculty Award from the KU School of Engineering and the President's Award from the City University of Hong Kong. Along with his coauthors, he won best paper awards of IEEE TRANSACTIONS ON COMMUNICATIONS (2016 Stephen O. Rice Prize) and IEEE PIMRC 2012. He is currently an Associate Editor of the IEEE TRANSACTIONS ON COMMUNICATIONS and previously served as a Guest Editor of IEEE TRANSACTIONS ON INDUSTRIAL INFORMATICS.

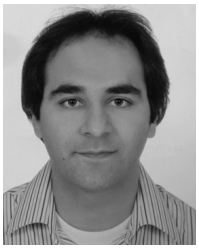

HADI GHAUCH (Member, IEEE) received the M.Sc. degree from Carnegie Mellon University, Pittsburgh, PA, USA, in 2011, and the Ph.D. degree in electrical engineering from the KTH Royal Institute of Technology, Stockholm, Sweden, in 2017. Since 2018, he has been an Assistant Professor with the Department of Digital Communications, Telecom ParisTech, and the Institut Polytechnique de Paris. His research interests include optimization for large-scale learning, optimization for millimeter-wave communication, and the distributed optimization of wireless networks.